INTERNATIONAL ATOMIC ENERGY AGENCY
UNITED NATIONS EDUCATIONAL, SCIENTIFIC AND CULTURAL ORGANIZATION
INTERNATIONAL CENTRE FOR THEORETICAL PHYSICS
I.C.T.P., P.O. BOX 586, 34100 TRIESTE, ITALY, CABLE: CENTRATOM TRIESTE

SMR.550 - 21

SPRING COLLEGE IN MATERIALS SCIENCE ON
"NUCLEATION, GROWTH AND SEGREGATION IN MATERIALS SCIENCE AND ENGINEERING"
(6 May - 7 June 1991)

STABILITY OF MICROSCOPIC CLUSTERS

(PART IV)

J.A. ALONSO
Departamento de Fisica Teorica y Fisica Atomica
Molecular y Nuclear
Facultad de Ciencias
Universidad de Valladolid
47011 Valladolid
Spain

STABILITY OF MICROSCOPIC CLUSTERS

4th Lecture: Microalloys

J. A. ALONSO

Lectures to be delivered at:
Spring College in Materials Science on
"Nucleation, growth and segregation in Materials Science and Engineering"
(International Centre for Theoretical Physics, Triestre, May-June 1991)

1. IMPURITIES IN SIMPLE METAL CLUSTERS[1]

Abundance maxima in pure alkali metal clusters have been explained by a spherical jellium model (see 2nd Lecture of this series). The ordering of the electronic energy levels in this model is 1s, 1p, 1d, 2s, 1f, 2p, 1g, ... Relative stability maxima are then predicted and observed for closed shell clusters. This occurs at N_e = 2, 8, 18, 20, 34, 40, 58, ... where N_e is the number of valence electrons in the cluster. This is also the number of atoms in neutral alkali clusters since alkali atoms are monovalent.

The spherical jellium model explains the magic numbers exclusively in terms of the electronic structure. In order to test further the validity of the jellium model and to shed light on the possible influence of the geometric structure, several abundance measurements have been performed for heteroatomic clusters, formed by atoms of different valence[2,3]. If only electronic structure controls the magic numbers, it is expected that abundance maxima (or drops in the ionization potential) will occur again for closed electronic shells.

By supersonic expansion of mixed vapours Kappes and coworkers[2,3] have obtained clusters containing a small amount of impurity atoms. In particular I concentrate here on a series of clusters with formula A_N B, that is, the cluster contains N atoms of type A (alkali element) and a single impurity atom of type B (monovalent of divalent). The particular systems under study are listed in Table 1, along with the experimentally observed abundance maxima in the small size range. The order chosen for the list in the Table is that of increasing value of $\Delta n_+ = n_+(B) - n_+(A)$, where $n_+(B)$ and $n_+(A)$ are the jellium density parameters of pure metals B and A respectively; for instance,

$$n_+(A) = \frac{Z(A)}{\Omega(A)} \qquad (1)$$

where Z(A) is the valence of element A and Ω is its volume per atom in the pure metallic state.

The main feature from the data reported in the Table is the observation of a new magic number, corresponding to ten valence electrons, for a large enough value of Δn_+. This new magic number begins with the system Na/Mg in this list. Associated with the occurrence of N_e = 10 is the disappearance of N_e = 18 as magic number. This occurs earlier in the list.

This experimental data was originally used by the experimentalists to criticize the jellium model. In effect, a naive application of the jellium model leads to disagreement with the experimental results in Table 1 since N_e = 10 can not be explained. Baladrón and Alonso[1], have demonstrated that a modification of the jellium model, to account for the different nature of the impurity, explains perfectly the experimental results. In fact, the origin of the new magic number is "again" a shell-effect.

The presence of an impurity atom induces, in general, a strong perturbation of the electronic cloud of an alkali cluster. The different nature of the foreing atom can be accounted for by a simple extension of the jellium model. The foreing atom is placed at the cluster centre and each subsystem (impurity and host) is characterized by its own ionic density in a jellium description, The following positive-charge background is then assumed

$$n_+(r) = \begin{cases} n_+(B) & , \ r < R_B \\ n_+(A) & , \ R_B < r < R \\ 0 & , \ r > R \end{cases} \qquad (2)$$

Here $n_+(B)$ is the jellium density parameter of the B metal ($n_+(B) = Z(B)/\Omega(B)$), R_B is the Wigner-Seitz radius of metal B, that is, the radius of a sphere with volume $\Omega(B)$, and R is the cluster radius, easily obtained from $\Omega(A)$, $\Omega(B)$ and the number of atoms.

All values of $n_+(B) - n_+(A)$ in Table 1 are positive, that is, the impurity provides a more attractive potential than the host. As a consequence, the original separation between the 2s and 1d shells becomes reduced. This is because the s-type electrons have a considerable probability of being near the center of the cluster, where the potential has become more attractive; this enhances the stability of the 2s shell. This effect, which is shown in Fig. 1 for the cluster $Na_{39}Li$, becomes more pronounced as the attractive strength of the impurity increases. When this attractive strength is strong enough, the order of the 1d and 2s levels becomes reversed, leading to a new shell ordering 1s, 1p, 2s, 1d, different from that in the pure jellium model. Ten electrons lead to the filling of the first three shells $(1s)^2$ $(1p)^6$ $(2s)^2$, and then $N_e = 10$ suddenly appears as a magic number. Evidently, for this shell ordering the next magic number is $N_e = 20$, corresponding to the configuration $(1s)^2$ $(1p)^6$ $(2s)^2$ $(1d)^{10}$. In other words, the appearance of $N_e = 20$ is associated to the disappearance of $N_e = 18$.

A quantitative view of this effect is given in Figure 2, where we have plotted the stability function

$$S(N_e) = E(A_{N-1}\,B) + E(A_{N+1}\,B) - 2E(A_N\,B). \qquad (3)$$

Here S is written as a function of N_e, the number of valence electrons in the A_NB cluster; this number is given by $N_e = NZ(A) + Z(B)$. The clusters $A_{N-1}B$ and $A_{N+1}B$ differ from A_NB by one host atom, and then by one

electron, since Z(A) = 1. The cluster energies needed to evaluate $S(N_e)$ from eq. (3) have been calculated by the same density functional technique used for pure metal clusters (see 2nd Lecture). At the top of Fig. 2 we have the system Na/Ba. Δn_+ is very small in this case (see table 1) and the order of the shells is the usual one of the standard jellium model. As the attractive power of the impurity atom increases we observe that the peak for $N_e = 18$ first decreases in magnitude and then disappears. This is so because the 2s level becomes so close to the 1d level that the gap separating these levels becomes zero. Finally, by increasing even further the attractive strength of the impurity the 2s shell becomes more stable than the 1d shell, giving rise to the new shell closing numbers. The peak at $N_e = 10$ appears just at Na/Mg, like in the experiment

2. MIXED CLUSTERS: MICROALLOYS

In the previous section I have considered the case of a single impurity atom immersed in a cluster of a simple metallic element. In the present Section I will consider the case of a cluster of general composition A_NB_M where A and B are two different metallic elements and N and M are the number of A-type atoms and B-type atoms, respectively, in the cluster. This is a complicated system, and only cases where both A and B are simple metals have been studied theoretically. Experimental work on microalloys in also scarce. Some interesting results have been obtained using a theoretical method called Spherically Averaged Pseudopotential (SAPS) model. So, first of all I describe this model, leaving the applications to microalloys for the last part of this Section.

2.1. The SAPS model

We have already seen in Section 1 of this Lecture that the simple jellium model must be modified in order to obtain meaningful results in the case of clusters containing impurities. A first-principles quantum chemical approach is not practical for large clusters, so intermediate methods between those two extremes (jellium and ab initio quantum chemistry) can be very helpful. One of such intermediate methods in the Spherically Averaged Pseudopotential model[4]. In this method the cluster is composed of a) ions and b) external (or valence) electrons. The idea of the method is to calculate the geometry of the cluster (that is, the positions of all the atoms) at temperature T = 0K, by minimization of the total energy of the cluster with respect to the 3N parameters representing the 3N coordinates of the N atoms forming the cluster. To achieve this formidable task one uses the Density Functional Formalism[5,6] and some drastic approximations. One of the approximations is:

i) The ions are substituted by effective pseudopotentials; in most applications by the empty core pseudopotential[7]:

$$V_{ec}(r) = \begin{cases} 0 & , \quad r < r_c \\ -\dfrac{Ze}{r} & , \quad r > r_c \end{cases} \qquad (4)$$

r_c is the empty-core radius and Z is the valence of the ion. This means that the attraction of the outer electrons by the ion is purely coulombic outside a sphere of radius r_c and zero inside.

If the set of ionic positions is represented by $\{\vec{R}_i\}$ then the total ionic potential seen by a valence electron at a point $\vec{r}$ of the cluster is

$$V_{ion}(\vec{r}) = \sum_{i=1}^{N} V_{ec}\left(|\vec{r} - \vec{R}_i|\right) \qquad (5)$$

where, for simplicity, the notation used assumes that all the N atoms of the cluster are equal (the extension to heteroclusters is trivial).

Eq. (5) provides a three-dimensional potential. The process of calculation of the cluster geometry starts by generating an initial geometry, represented by an initial set of nuclear positions $\{\vec{R}_i\}_{initial}$. The Kohn-Sham equations of the Density functional formalism (see 2nd Lecture) are then solved self-consistently to obtain the electron density of the cluster and then its total energy. Since the initial geometry was chosen arbitrarily, small displacements of the ions from their initial positions can lower the total energy of the cluster. Another way to state this is that the forces acting on the atoms are not zero for this initial configuration. This indicates what should be done next. Each atom is moved a small distance precisely in the direction of the net force acting on it. This process generates a new set of ionic positions $\{\vec{R}_i\}$. Now, the total energy of the cluster is calculated for the new geometry. The cycle is repeated again and again until all the forces vanish, that is, until the energy of the cluster is at the bottom of a (relative) minimum. Since we want to obtain the geometry corresponding to the absolute energy minimum we repeate the whole precess just described from the very begining, that is, we start with a new set $\{\vec{R}_i\}_{initial}$ of "initial" ionic coordinates. Evidently trying many initial configurations we have more chances of finding the true absolute equilibrium geometry, or at least one with an energy rather close to it.

In the way I have described the process of finding the cluster geometry, I have avoided mentioning the second, rather strong, simplification introduced in the SPAS calculations:

ii) The total ionic potential $V_{ion}(\bar{r})$ given by eq. (5) is replaced by its spherical average $V_{ion}^{av}(r)$ about the cluster centre:

$$V_{ion}(\bar{r}) \rightarrow V_{ion}^{av}(r) . \qquad (6)$$

This simplification drastically reduces the computational difficulties since we now have a problem of interacting electrons moving in an external potential well with spherical symmetry. Despite this simplification the SAPS method goes a long way beyond the jellium model, since:

a) The ionic potential is less smooth than the external potential of the jellium model. This can be appreciated in Fig. 3, which shows the total electrostatic potencial, ionic plus electronic, for several Aluminium clusters[8].

b) Although the ion-electron interaction only keeps the radial part of the total ionic potential, the ion-ion interaction $E_{ion-ion}$ is calculated considering the true three-dimensional array of ions, that is

$$E_{ion\text{-}ion} = \sum_{i \neq j} \frac{(Z_i)\,(Z_j)\,e^2}{|\bar{R}_i - \bar{R}_j|} \qquad (7)$$

2.2 Results of the SAPS model for pure clusters

Before considering the case of hetoroclusters we show some results obtained for clusters of a single metallic element.

Figure 4 shows the radial distribution of atoms in Na_{25} and Na_{30}. This result illustrates one of the main conclusions: the clusters are composed of shells of atoms. At this small size, most ot the atoms are in the outer, or surface shell, and only a few atoms are in the inner shell. The outer shell shell has a width of nearly one atomic unit. The evolution of the population of the inner and outer shells is displayed in

Figure 5 for the case of Cs_N. Very small clusters have only one shell with its centre empty. Between N = 7 and N = 18 the centre is occupied by one atom. The population of the inner shell increases slowly after N =18 and the geometrical centre of the cluster becomes empty again . At N = 40 one atom occupies the center of the cluster and the configuration of a central atom plus two surrounding atomic shells persists until N = 64, where a third shell begins to grow in the inner region of the cluster.

In conclusion, we observe a strong reconstruction of the cluster geometry as it grows. Also we observe that new atomic shells grow in the innermost region of the cluster when there is enough free space to accomodate first one single atom and then additional atoms. There is a complementary view of this effect. Between Cs_7 and Cs_{18} the distance between the central atom and the surface atoms increases slowly since more atoms must be accomodated in the surface layer. For Cs_{18} this distance has become slightly larger than the nearest-neighbor distance in metallic Cs, $d_{nn}^{bulk} = 9.893$ a.u. The SAPS calculation indicates that Cs_{19} reconstructs its geometry to avoid interatomic distances larger than d_{nn}^{bulk}. This is achieved by placing the added atom in the interior of the cluster, instead of placing it on the surface. For Cs_{63} the situation is analogous. Now the central atom is surrounded by an atomic shell of 19 atoms at a mean radius nearly identical to that of Cs_{18} and again larger that d_{nn}^{bulk}. The next cluster, Cs_{64}, has two atoms in the innermost region, like Cs_{19}.

Other result we have found is a contraction of the cluster volume with respect to that of an equivalent piece of bulk metal. This is shown in Figures 6 and 7 for Al and Cs clusters, respectively. What these figures show is that the calculated cluster radius is smaller that the

radius assumed in the jellium model (in the jellium model the volume is the same as that of an equivalent piece cut from a macroscopic metal. This global contraction of the cluster volume seems to be a general feature in small metallic clusters, and is well documented experimetally[11]. We have recently shown[10] that the volume contraction explains the discrepancies found between experiment and jellium calculations concerning the static polarizabilities of small aluminium clusters[12]. Specifically, the measured polarizabilities of Al_N clusters with N<40 are smaller than those predicted by a jellium calculation. The classical polarizability (per atom) for a metallic sphere of radius R is

$$\alpha_{classical} = \frac{R^3}{N} \quad . \tag{8}$$

For a jellium sphere the polarizability is enhanced because the electronic charge density spills out beyond the jellium radius, and the polarizability can be written[13]

$$\alpha_{Jellium} = \frac{(R+\delta)^3}{N} \tag{9}$$

where δ, which is related to the electronic spill out, is small and approximately constant for all sizes. The fact that the jellium polarizabilities of small Al clusters are larger than the experimental ones indicates, evidently, that R is overestimated in the jellium model. Since the SAPS calculation decreases the value of R, it leads to better polarizabilities[10].

In the 2nd Lecture of this series we described the work of Martin and coworkers and how these authors modified the jellium model in order to obtain the required sequence of magic numbers (reflected in the sudden drops of the ionization potential) for clusters of alkali metals. Success was achieved by deforming the positive charge

background to make the cluster denser in its inner part. SAPS calculations[14] have provided a microscopic interpretation of the model used by Martin and coworkers. An analysis of the interatomic distances in Cs_N clusters with sizes up to N = 80 shows that the contraction of interatomic distances is not a homogeneous one. Distances in the inner region of the cluster are more compressed than in the outer region. This finding gives support to Martin's model. Furthermore, additional calculations for Mg clusters[15] indicate the same effect. In summary, the inhomogeneous contraction of interatomic distances seems to be a general effect in simple metal clusters.

2.3 SAPS model for clusters with a single impurity[9,16]

The case of Cs clusters with a single Oxigen impurity has been studied in detail. Experimental results also exist for this system[17]. Studies of the interaction of Cs with O exhibit a technological aspect, since oxidized thin films of Cs have very low work functions and are therefore applied as photocathodes. Here we will be concerned with the question how the embedding of a highly reactive impurity like oxigen in an alkali-metal cluster changes the size-dependent electronic and structural properties of the host cluster.

The only relevant comments about how the SAPS calculation is performed in this particular case are the following ones: a) The cluster centre is identified with the position of the Oxigen nucleus. b) The inner electrons of the Oxigen atom are also included in the calculation.

Figure 8 shows the one-electron energy eigevalues of the system Cs_NO as a function of N. The electronic configuration of the free oxigen atom is $(1s)^2\ (2s)^2\ (1p)^4$. We observe in the figure that the 1p shell is the first to be filled by the valence electrons of the Cs atoms. The sequence of shells is 1p, 3s, 2p, 1d, 1f, 4s, 3p, 1g, 2d, ... This sequence

results in closed-shell configurations at N = 2, 4, 10, 20, 34, 36, 42, 60. The onset of the 4s shell is practically degenerate with 1f and the same occurs for 1g and 3p. In conclusion, pronounced shell closing effects only occur for N = 10, 20, 36 and 60 (excluding very small sizes). These effects become reflected in the calculated ionization potentials (figure 9). The qualitative features of the experimental data agree quite well with the calculation: the predicted drops at N = 10, 20, 36 show up clearly in the experimental data. In summary the Oxigen atom in Cs_NO clusters forms and ion O^{2-} and the remaining N-2 valence electrons of the cluster behave in the simplest way, that is, these give rise to shell effects. The experimental[17] information indicates that an analogous effect occurs for clusters with more oxigen atoms. That is, in clusters of composition Cs_NO_X there are N-2x free-electron-like electrons.

A second aspect of interest concerns the structural effects induced by the presence of the Oxigen impurity. The strong ionic bonding between the impurity and the Cs atoms produces a rearrangement of the inner part of the Cs_N cluster after the introduction of the impurity. We can distinguish two cases. If the central site in Cs_N is empty (for instance from Cs_{19} to Cs_{39}) the introduction of the Oxigen atom produces only a small rearrangement of the innermost Cs shell: the radius and the population of this shell changes only slightly (see, for instance, figure 10. In contrast, when the central site is occupied in Cs_N, then the structural rearrangement is drastic. The case of N = 60 given in fig. 10 shows what happens: a few Cs atoms (in most cases six atoms; see below) are splitted from the outer part to form a Cs shell directly surrounding the oxigen impurity. The radius of this shell is about 5 a.u. The radius of the first coordination shell around a central

Cs atom in a pure Cs_N cluster is much larger (see figure 7). The reason for this difference is that the atomic size of Cs is larger than that of Oxigen and Cs needs a larger hole to be accomodated.

Also related to this fact is the observation that there is a maximum of 10 Cs atoms around the Oxigen atom. This number is smaller than in pure Cs_N where we find up to 19 atoms surrounding a central Cs atom. The details of the population of the shell surrounding the oxigen atom, as well as the population of other more external shells, are given in Figure 11. The radii of those shells are given in Fig. 12. The population of the first coordination shell around the oxigen atom is remarkably stable (the set of clusters $Cs_{35}O$ to $Cs_{46}O$ are exceptions); this shell is a group of six Cs atoms forming an octahedral arrangement around O. As a consequence, the radius of this shell is also very stable. Figure 13 shows the structure of $Cs_{14}O$, which exhibits eight second nearest neighbors in cubic coordination around the Cs_6O core. Both the sixfold coordination and the bond length in the Cs_6O core agree with the corresponding properties of solid Cs_2O, which is the only known oxidic solid with Anti-$CdCl_2$ structure.

The calculated embedding energy $\Delta H(N)$ of oxigen in Cs_N clusters is presented in Fig. 14. The embedding energy is negative for all N, showing a strong affinity of Cs_N for oxigen. $\Delta H(N)$ exhibits an oscillatory behavior around a mean value of approximatelly 0.43 a.u. This oscillatory behavior can be easily understood: the immersion of oxigen is favoured if the central position in the Cs_N cluster is empty and hindered if it is already occupied. In the first case one expects optimal conditions if the first shell of Cs atoms around the empty central site just contains six atoms, since then the stable Cs_6O core

can easily be formed. From Fig. 6 we see that this situation just happens at N = 6 and around N = 30.

2.4 Microalloys

We now turn to the case of mixed clusters of general composition $A_m B_n$. The experimental information on those systems is scarce, although some observations have been made in selected systems: for instance, Kappes and coworkers have found that by co-expansion of a mixed vapour of Li and Na the clusters formed are enriched in Li with respect to the initial composition of the mixed atomic vapour[3]. From the theoretical side, calculations using the Car-Parrinello method (a method which combines density functional and molecular dynamics ideas) have found segregation of potassium to the surface of a $Na_{10}K_{10}$ cluster[18]. Segregation in bulk alloys is a well studied topic[19]. Segregation theories predict that Cs should segregate to the surface of a liquid Na-Cs alloy. This result is supported by Monte Carlo simulations[20].

The SAPS method has been applied to Na-Li and Na-Cs clusters with varying composition[21,22]. The only difference with respect to the calculation for a single component is that we now have two different kinds of ionic pseudopotential: one for Na and another for Li (or Cs). Taking again the empty core pseudopotential, each element has its own empty core radius.

We first consider the main fatures of the atomic distribution in $Na_m Cs_n$ with m=n and m=2n, and a total number of atoms m+n= N<90. A common characteristic for the two concentrations is the formation of homoatomic shells, that is, separated shells of Na and Cs atoms, respectively, with the most external shell always occupied by Cs atoms.

The most salient features concerning the formation and evolution of these shells with cluster size can be observed in Figure 15.

a) Clusters up to about N=42 have two homoatomic layers, the inner one formed by Na atoms and the outer one by Cs atoms. The Na layer is less well defined than the Cs layer, this one being appreciably thinner. For $Na_{2n}Cs_n$ there is and broadening of the Na shell with respect to the Na_nCs_n. This is an effect of the different relative concentration.

b) Larger clusters, 46 ≤N≤60, develop a Cs layer in the inner region of the cluster. Then, their configuration is that of a Na region with a large dispersion of radial distances, bounded on the inside by a Cs shell and on the outside by another, more populated, Cs shell. This Cs-Na-Cs stratification can be considered as a precursor to superlattice formation in the bulk solid alloy (the only stable bulk intermetallic compound has the Na_2Cs composition[23]). Notice that the atom distribution in $Na_{60}Cs_{30}$ suggests that a new Na shell is growing in the central region of the cluster, leading to an stratification Na-Cs-Na-Cs.

The segregation and stratification effects found for Na-Cs clusters are evidently due to the different radii of the empty-core pseudopotential: r_{ec}(Na) = 1.74 a.u., r_{ec}(Cs)=2.74 a.u. Cs segretates to the surface because this lowers the surface energy.

A second system where we have studied mixing and segregation effects is Li/Na[23]. Several radial distributions of atoms about the cluster center are given in Figure 16. In contrast to the Na/Cs case we observe more mixing. Notice that the external shell contains both Na and Li atoms. However the outermost part of this shell is enriched in Na. We conclude that the segregation effect is rather general, although its intensity varies (it is more pronounced in Na/Cs, where the surface shell is purely Cs, than in Na/Li).

One can ask to what extent segregation or ordering effects influence the magic numbers of abundance, well established for homoatomic alkali clusters. We do not know of any experiment performed for Na-Cs clusters. The system Li-Na has been studied by Kappes et al[3]. These authors have found abundance maxima for a number of electrons 8, 20, 40... irrespective of the relative concentration of Li and Na in the cluster (see Fig. 17). This suggests that even in mixed alkali clusters electronic effects are much more important than the structural effects associated to the cluster geometry. Fig. 18 shows the calculated energy per atom in Na_nCs_n as a function of cluster size. This function shows pronounced minima for a number of atoms equal to 8, 20, 40 and 58. We then predict that these clusters should be prominent in the abundance spectrum. The same prediction is obtained for Li/Na clusters[24], which evidently is in perfect agreement with experiment. The conlusion is that shell effects are also relevant in mixed alkali clusters.

We close this section with two final observations. The first one refers to the enrichment effect observed in the coexpansion of Li and Na vapours to form mixed Na/Li clusters (this effect is also observed for K/Na[25]): the clusters are enriched in the lighter alkali metal, compared to the original concentration in the mixed vapour. It has been proposed[3] that the Na/Li clusters detected are formed after many cycles involving atom aggregation, atom evaporation and reactions of substitution of a Na atom by a Li atom. To connect with the experimental results we have calculated the heat ΔH for the reaction of substitution of a Na atom by a Li atom

$$Na_{N-x+1}\,Li_{x-1} + Li \rightarrow Na_{N-x}\,Li_x + Na. \qquad (10)$$

This heat of reaction is

$$\Delta H = E(Na_{N-x}\,Li_x) + E(Na) - E(Na_{N-x+1}\,Li_{x-1}) - E(Li), \qquad (11)$$

written in terms of cluster energies. The results have been plotted in fig. 19 for several values of x. The most important observation is that ΔH is always negative, that is, substitution of a Na atom by a Li atom is favorable. This, in our view, explains the enrichment effect observed in the experiments.

The last observation concerns the comparison of the structures of Na_n and Na_nCs_n. These are given in Figure 20. The geometry of the Na_n core in $Na_n\,Cs_n$ is different from that of pure Na_n. The mechanism of reconstruction is the formation of a polyhedron with a number of faces consistent with the number of external Cs atoms; the Cs atoms sit on top of those faces.

REFERENCES

1. C. Baladrón and J.A. Alonso, Physica B 154, 73 (1988)
2. M.M. Kappes, M. Schär, C. Yeretzian, U.Heiz, A. Vayloyan and E.Schumacher, in: Physics and Chemistry of Small Clusters, NATO ASI Series B, Vol 158, Eds. P. Jena, B.K. Rao and S.N. Khanna, Plenum, New York (1987) p. 263
3. M.M. Kappes, M. Schär and E. Schumacher, J. Phys. Chem. 91, 658 (1987)
4. M.P. Iñiguez, M.J. López, J.A. Alonso and J.M. Soler, Z. Phys. D 11, 163 1989)
5. Theory of the inhomogeneous electron gas, Ed. S. Lundqvist and N.H. March, Plenum, New York (1983)
6. R.G.Parr and W. Yang, Density Functional Theory of Atoms and Molecules. Oxford Univ. Press, Oxford (1989)
7. N.W. Ashcroft, Phys. Lett. 23, 48 (1966)
8. C. Baladrón, M.P. Iñiguez and J.A. Alonso, Z. Phys. B, 59, 187 (1985)
9. U. Lammers, G. Borstel, A. Mañanes and J.A. Alonso, Z. Phys. D 17, 203 (1990)
10. A. Rubio, L.C. Balbás and J.A. Alonso, Solid State Commun. 75, 139 (1990)
11. C. Solliard and M. Flueli, Surf. Sci. 156, 487 (1985)
12. W.A. de Heer, P. Milani and A. Châtelain, Phys. Rev. Lett. 63, 2834 (1989)
13. D.R.Snider and R.S. Sorbello, Phys. Rev. B 28, 5702 (1983)
14. A. Mañanes, J.A. Alonso, U. Lammers and G. Borstel, submitted for publication.
15. M.D. Glossman, M.P. Iñiguez and J.A. Alonso, submitted for publication
16. U. Lammers, A. Mañanes, G. Borstel and J.A. Alonso, Solid State Commun. 71, 591 (1989)

17. T. Bergmann, H. Limberger and T.P. Martin, Phys. Rev. Lett. 60, 1767 (1988)
18. P. Ballone, W. Andreoni, R. Car and M. Parrinello, Europhys. Lett. 8, 73 (1989)
19. J.A. Alonso and N.H. March, Electrons in Metals and Alloys. Academic, New York (1989), Chapter 10
20. S.A. Rice, Z. Phys. Chem. 156, S 53 (1988)
21. M.J. López, M.P. Iñiguez and J.A. Alonso, Phys. Rev. B 41, 5636 (1990)
22. A. Mañanes, M.P. Iñiguez, M.J. López and J.A. Alonso, Phys. Rev. B 42, 5000 (1990)
23. M. Hansen and K.Anderko, Constitution of Binary Alloys. McGraw Hill, New York (1958)
24. M.J. López, M.P. Iñiguez and J.A. Alonso, Phys. Rev. B 41, 5636 (1990)
25. C. Brechignac and P. Cahuzac, Z. Phys. D 3, 121 (1987)

FIGURE CAPTIONS

Figure 1. The presence of an attractive impurity at the center of a Na cluster leads to a decrease in the gap between the 1d and 2s shells.

Figure 2. Second derivative of the cluster energy as a function of the number of valence electrons in the cluster

Figure 3. Total electrostatic potential (ionic plus electronic) for aluminium clusters with N = 23 (- · - · -), 31 (- - -) and 43 (———). The pronounced structure comes from the ionic part of the potential.

Figure 4. Calculated radial distribution of atoms in Na_{25} and Na_{30}. From Iñiguez et al[4].

Figure 5. Number of atoms in the various geometrical shells a-c of Cs_N clusters versus N. From Lammers et al[9].

Figure 6. Cluster radius (divided by $N^{1/3}$) versus cluster size N, for Aluminium clusters. From Rubio et al[10].

Figure 7. Radii of the various geometrical shells a-c of Cs_N clusters versus N. The dashed line is the cluster radius in the spherical jellium model. From Lammers et al[9]

Figure 8. One-Electron energy eigevalues for Cs_NO clusters versus N.

Figure 9. First ionization potential for Cs_NO clusters versus N.

Figure 10. Radial distribution of atoms and electronic densities (in appropriate units) for Cs_N and OCs_N with N=20, 26, 32 and 60. The stars indicate Cs atoms and the circle the oxigen.

Figure 11. Number of Cs atoms in the various geometrical shells a-c in Cs_NO clsuters versus N

Figure 12. Radii of the various geometrical shells a-c of Cs_NO clusters versus N

Figure 13. Calculated structure of $Cs_{14}O$

Figure 14. Embedding energy of oxigen in Cs_N clusters versus N.

Figure 15. Radial distribution of atoms (with respect to the center of ionic charge of the cluster. Stars indicate Cs atoms and circles Na atoms. The electron density is also plotted in appropriate units.

Figure 16. Radial distribution of atoms in different Na/Li clusters measured from the center of the cluster. Solid circles and crosses represent Li and Na atoms respectively.

Figure 17. Mass spectra for mixed Na/Li clusters.

Figure 18. Energy per atom in Na_nCs_n as a function of cluster size. Filling of electronic shells is indicated

Figure 19. Heat of the substitution reaction of a Na atom by a Li atom (eq. 11 of the text) for several values of x (x = 1, 2, 5 and 10). From ref. 24.

Figure 20. Geometries of Na_n(left-hand column), Na_n core in Na_nCs_n (central columm) and whole Na_nCs_n cluster (right hand column). Open and solid circles represent Na and Cs atoms respectively. Distances are in a.u.

Table I
Abundance maxima in heteroatomic clusters $A_N B$ produced in supersonic expansions. The abundance maxima are characterized by the number of valence electrons in the cluster. Also given is the difference Δn, in positive background density between the two metals (in the jellium model).

Metals (A/B)	Δn, (au)	Maxima
Na/Ba	0.0008	8, 18
Na/Sr	0.0014	8, 18–20
K/Na	0.0018	8, 20
Na/Eu	0.0023	8, 18
Na/Li	0.0029	8, 20
Na/Ca	0.0029	8, 20
Na/Yb	0.0033	8, 20
K/Li	0.0047	8, 20
Na/Mg	0.0088	8–10
K/Mg	0.0106	10, 20
K/Hg	0.0106	10, 21
Na/Zn	0.0155	10, 20
K/Zn	0.0173	10, 20

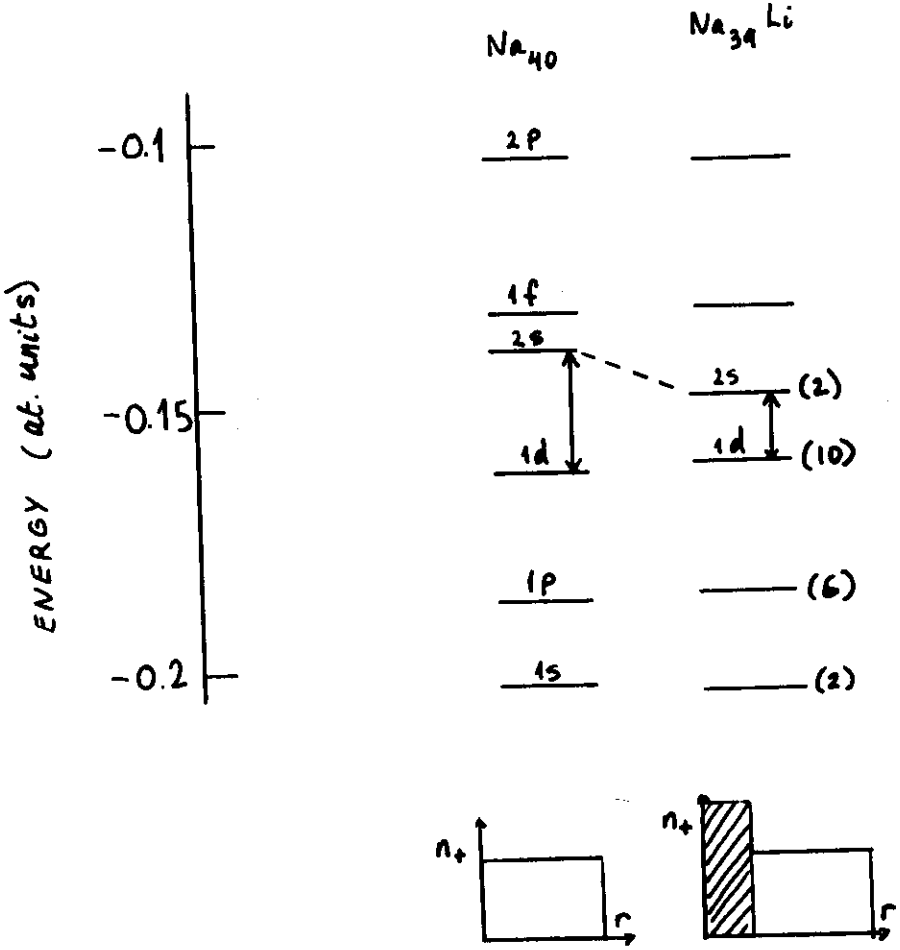

Fig. 1

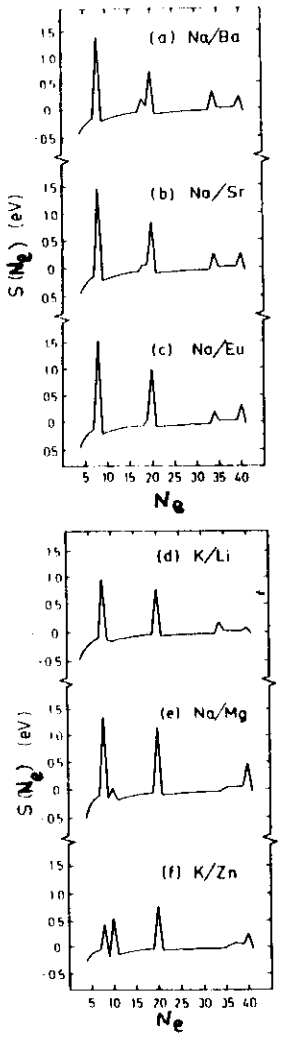
(a) Na/Ba
(b) Na/Sr
(c) Na/Eu
(d) K/Li
(e) Na/Mg
(f) K/Zn
S(Ne) (eV)
Ne

Fig. 2

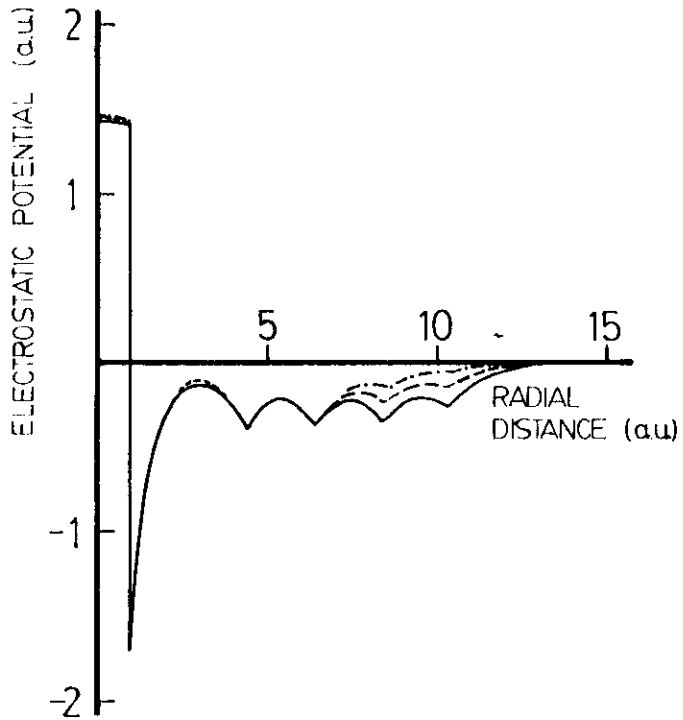
ELECTROSTATIC POTENTIAL (a.u.)
RADIAL DISTANCE (a.u.)

Fig. 3

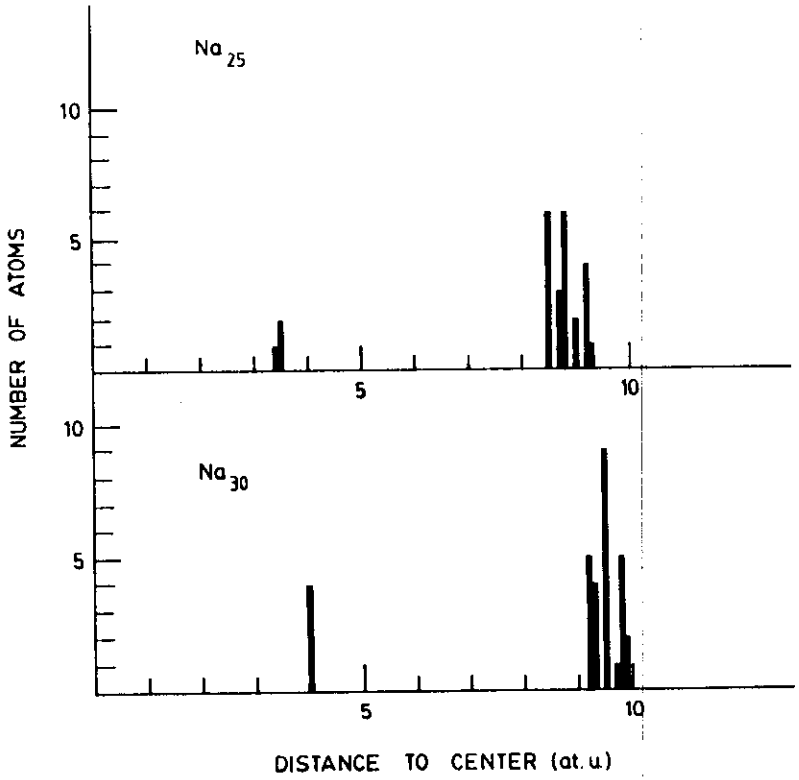
Na 25
Na 30
NUMBER OF ATOMS
DISTANCE TO CENTER (at.u.)
10
5
5
10
10
5
5
10

Fig 4

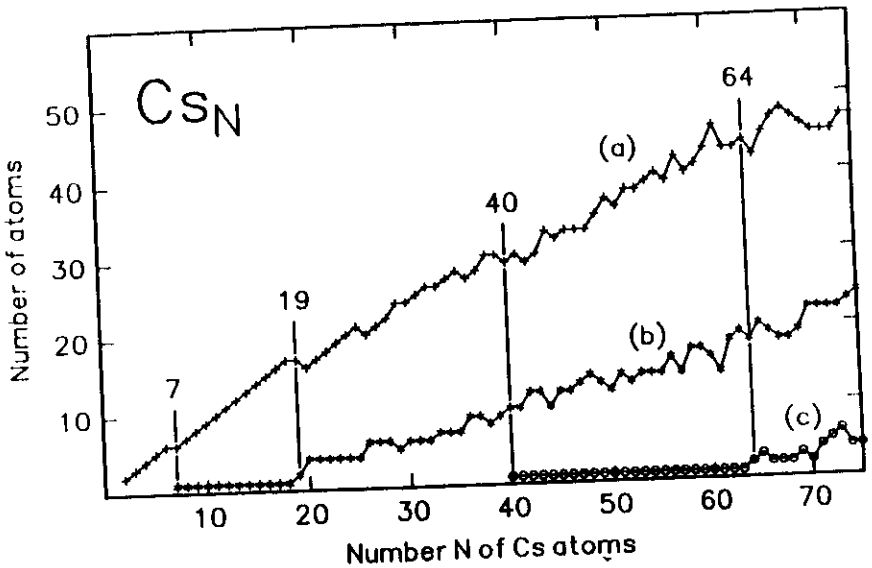
Cs N
Number of atoms
Number N of Cs atoms
(a)
(b)
(c)
7
19
40
64
10
20
30
40
50
60
70

Fig. 5

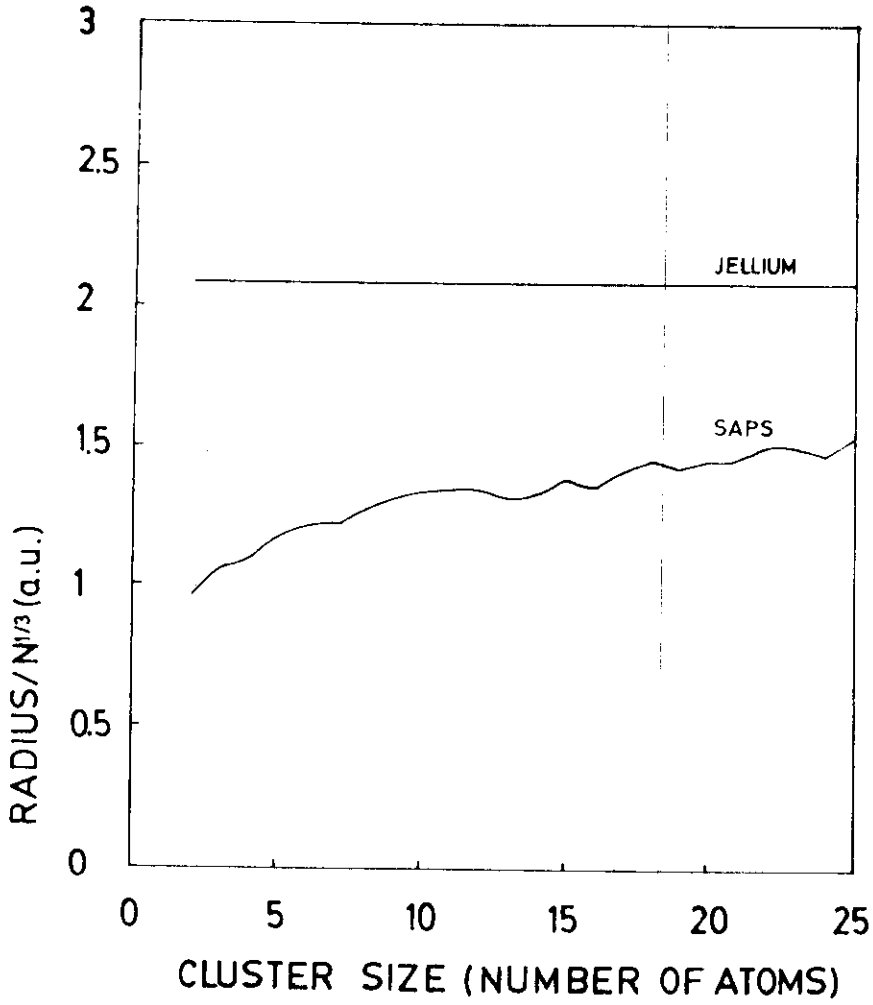
3
2.5
2
1.5
1
0.5
0
JELLIUM
SAPS
RADIUS/N^1/3 (a.u.)
0
5
10
15
20
25
CLUSTER SIZE (NUMBER OF ATOMS)

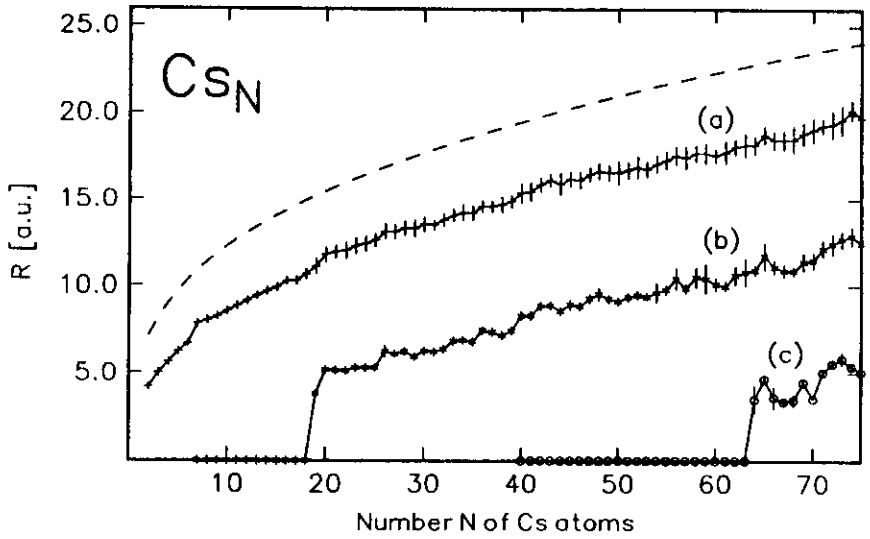
25.0
20.0
15.0
10.0
5.0
Cs_N
(a)
(b)
(c)
R [a.u.]
10
20
30
40
50
60
70
Number N of Cs atoms

Fig. 7

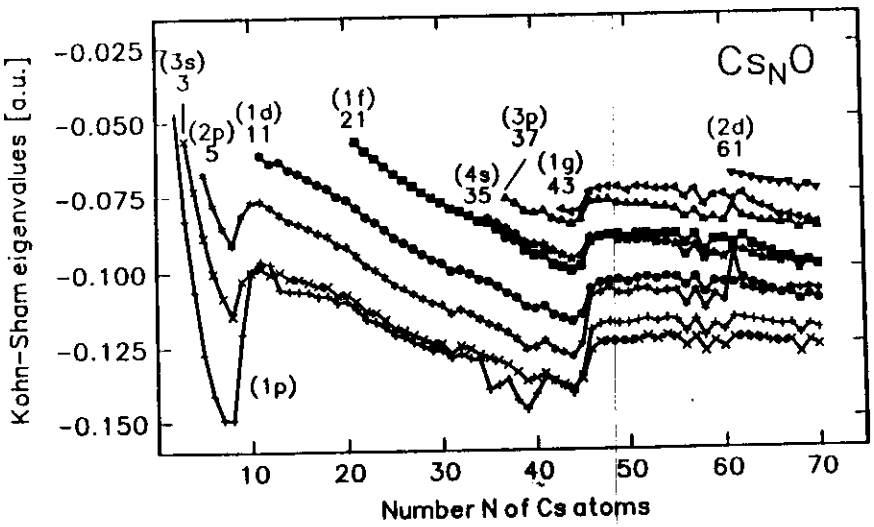

Fig. 8

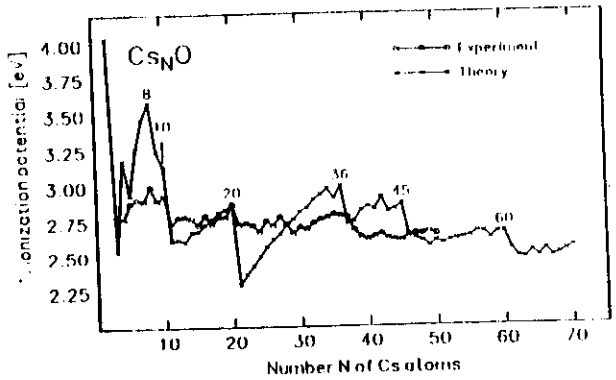

Fig. 9 First ionization potential for Cs_NO clusters versus N.

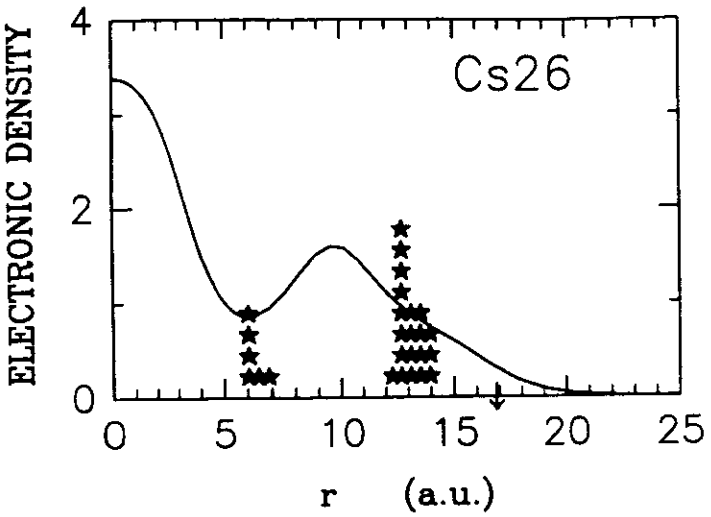
Cs26
ELECTRONIC DENSITY
r (a.u.)

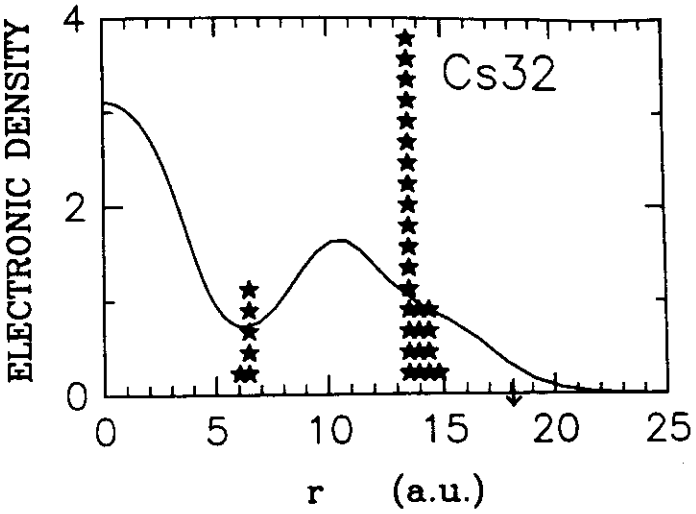
Cs32
ELECTRONIC DENSITY
r (a.u.)

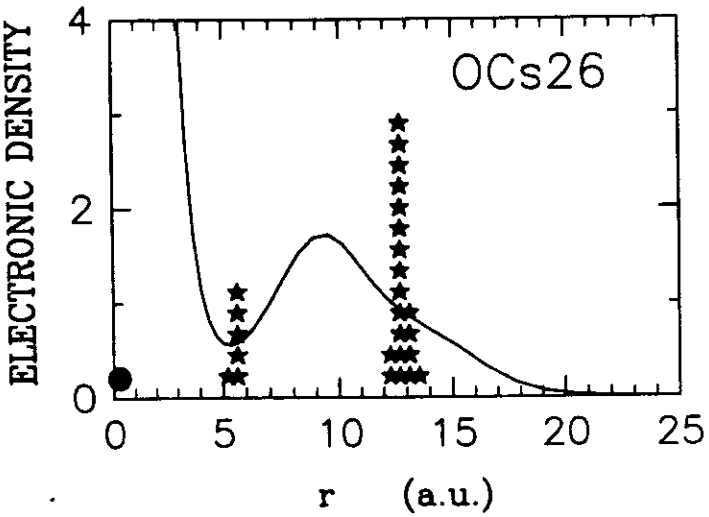
OCs26
ELECTRONIC DENSITY
r (a.u.)

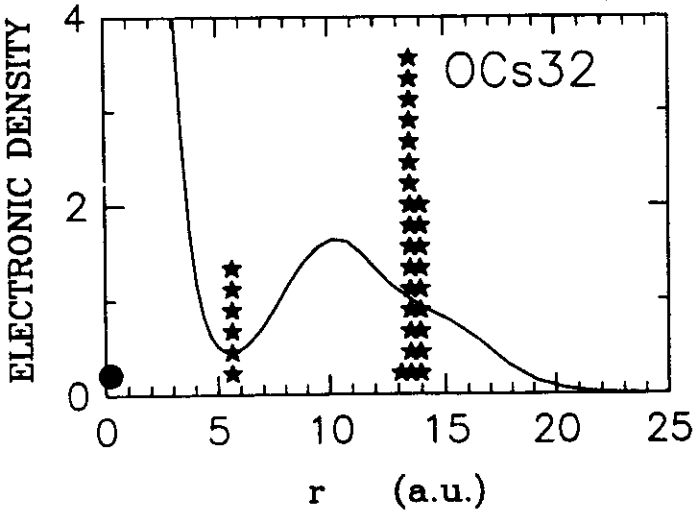
OCs32
ELECTRONIC DENSITY
r (a.u.)

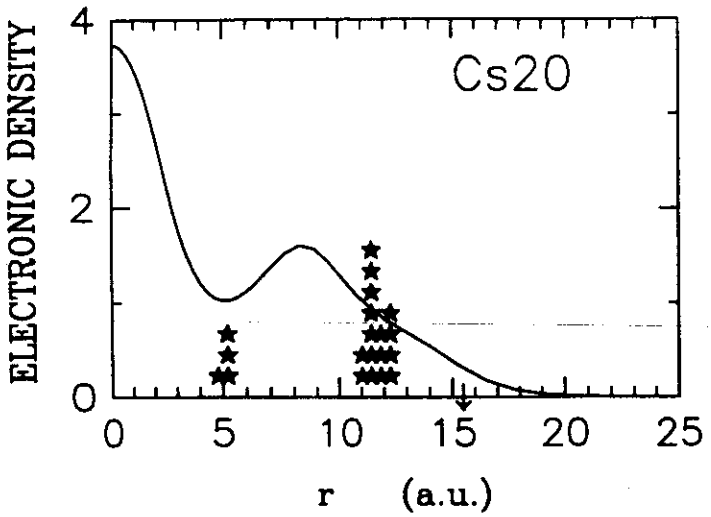
Cs20
ELECTRONIC DENSITY
r (a.u.)

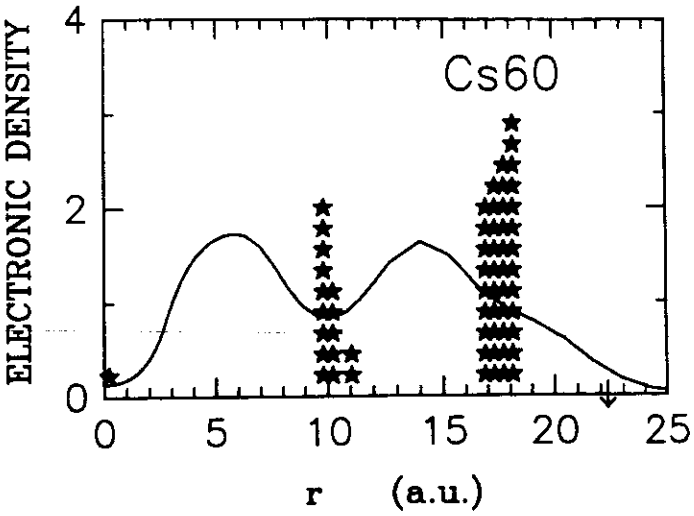
Cs60
ELECTRONIC DENSITY
r (a.u.)

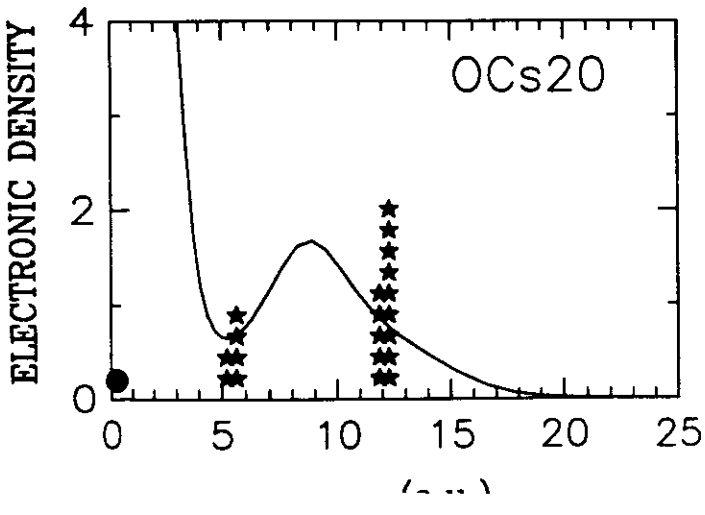
OCs20
ELECTRONIC DENSITY

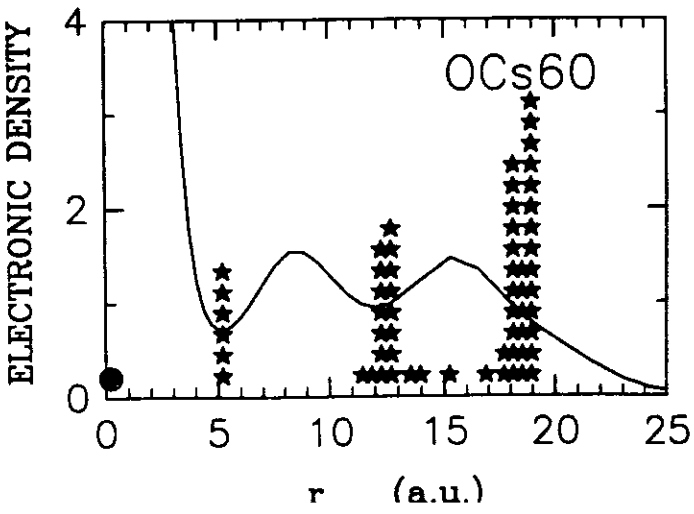
OCs60
ELECTRONIC DENSITY
r (a.u.)

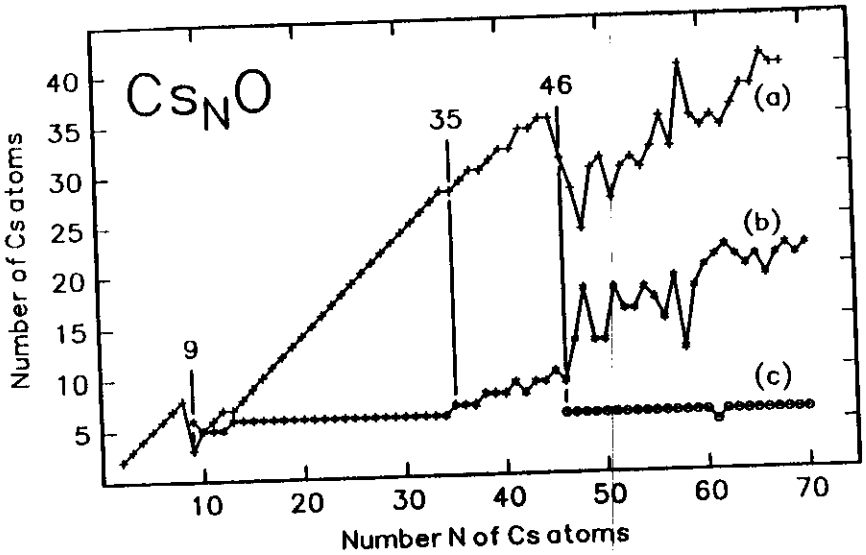

Fig. 11

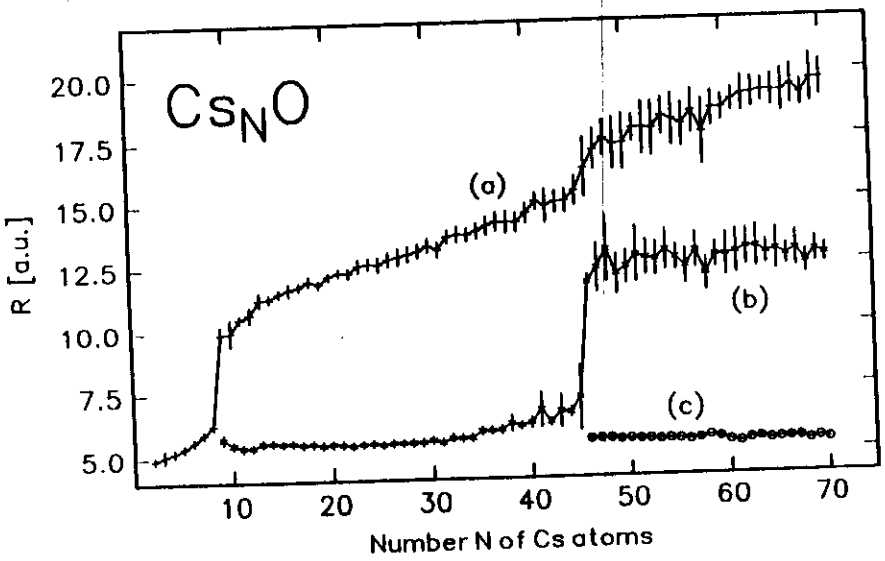

Fig. 12

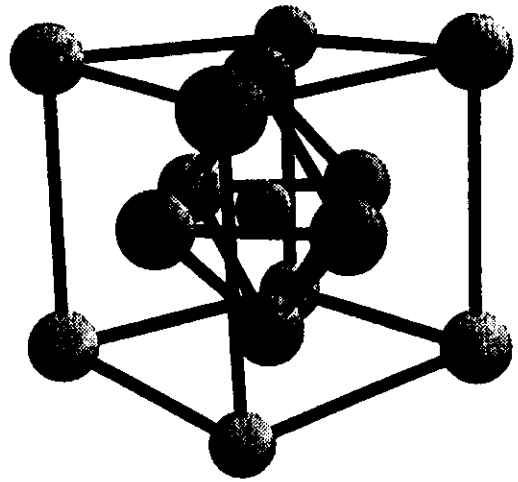

Fig 13

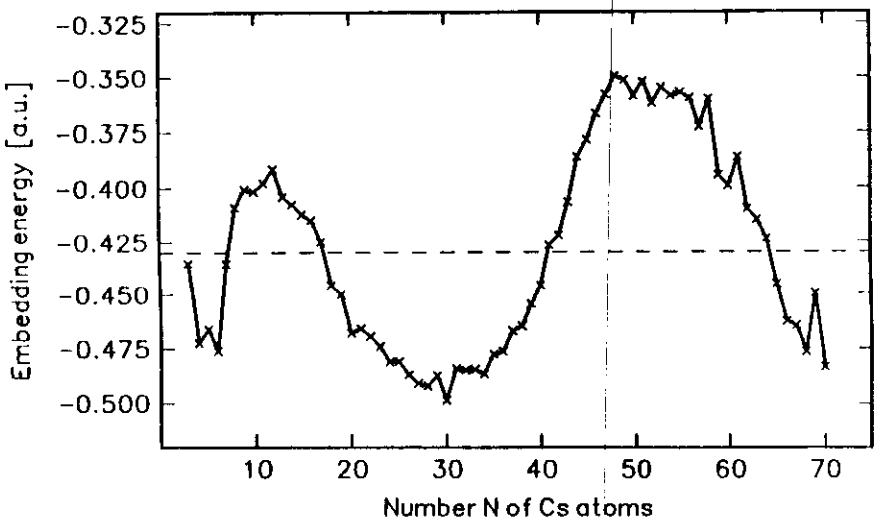
Embedding energy [a.u.]
-0.325
-0.350
-0.375
-0.400
-0.425
-0.450
-0.475
-0.500
10
20
30
40
50
60
70
Number N of Cs atoms

Fig 14

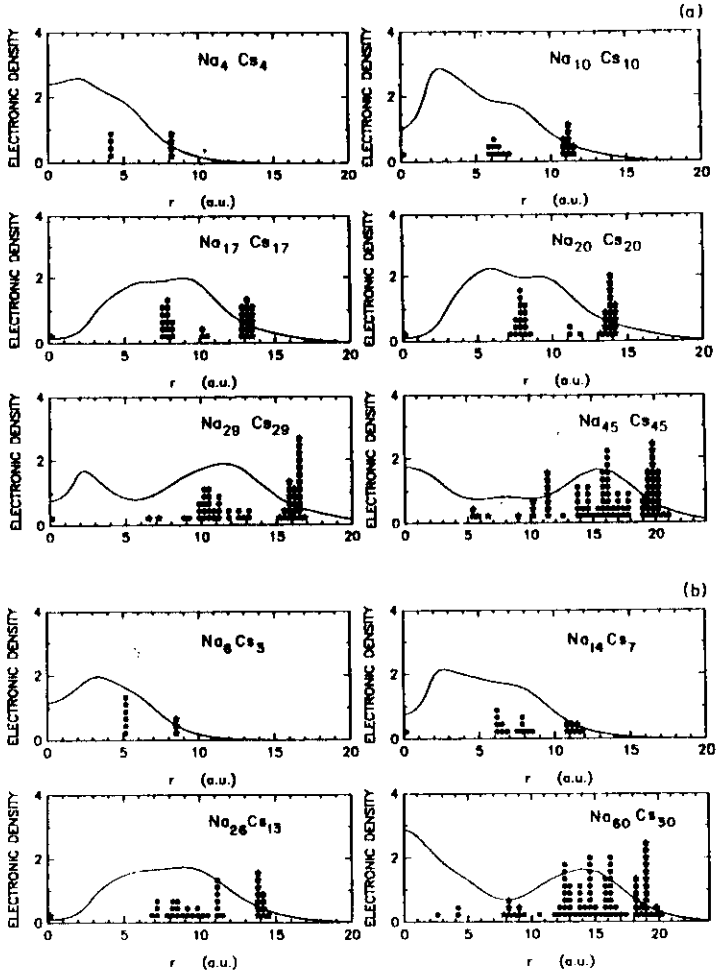
(a)
ELECTRONIC DENSITY
Na4 Cs4
Na10 Cs10
Na17 Cs17
Na20 Cs20
Na29 Cs29
Na45 Cs45
r (a.u.)
(b)
Na8Cs5
Na14Cs7
Na26Cs13
Na60Cs30

Fig 15

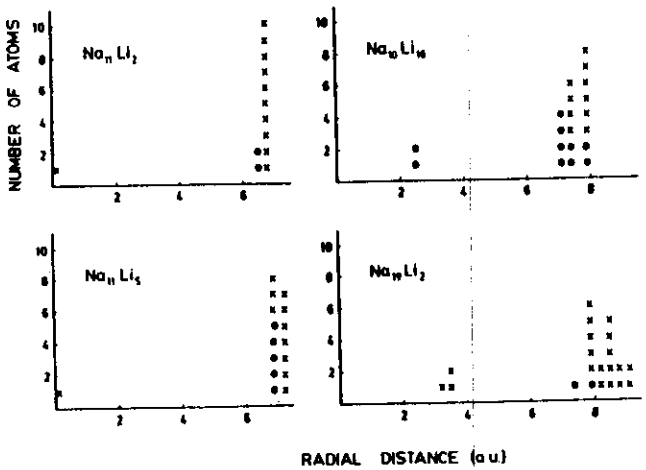

FIG. 16 Radial distribution of atoms in different Na_N , Li_x clusters, measured from the center of ionic charge of the cluster. Solid circles and crosses represent Li and Na atoms, respectively.

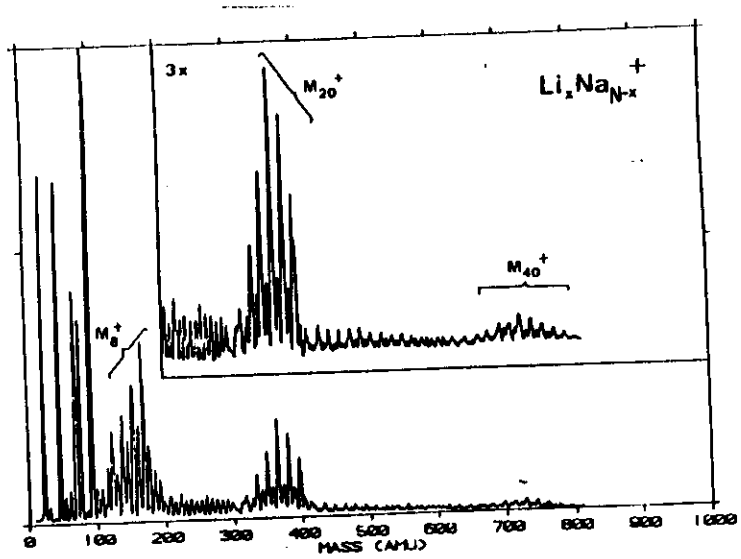

Fig. 17

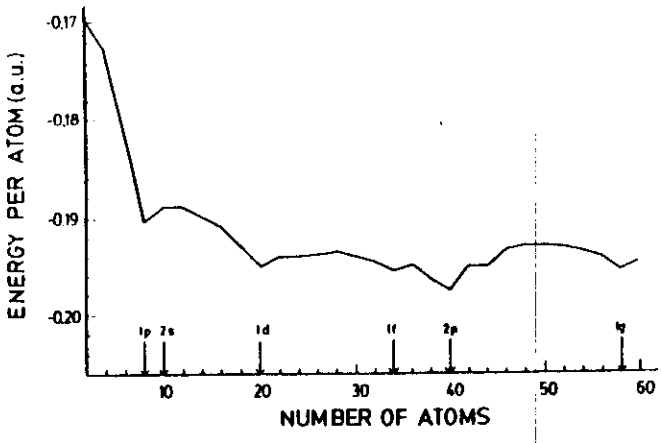

FIG. 18 Energy per atom, $E(N)/N$, in Na_nCs_n as a function of cluster size. Note that N has only even values. Filling of electronic shells is indicated.

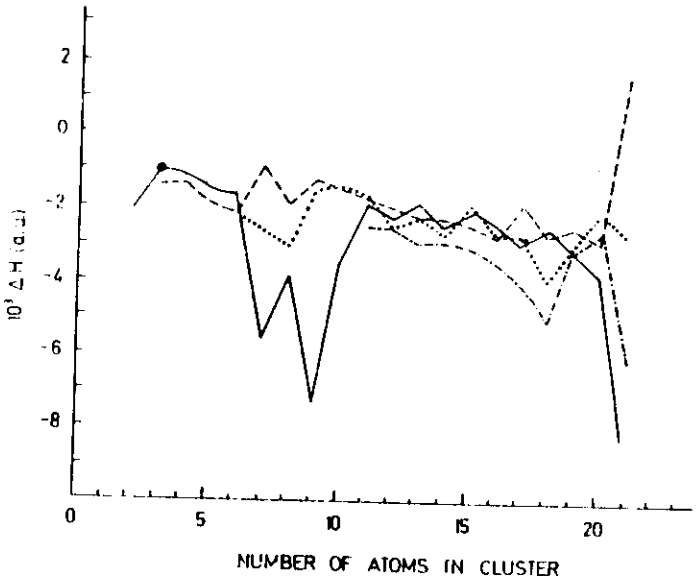

FIG. 19. Heat of the substitution reaction $Na_{N-x+1}Li_{x-1} + Li \rightarrow Na_{N-x}Li_x + Na$ for $x = 1$ (——), $x = 2$(– – –), $x = 5$(· · · ·), and $x = 10$(— · — · —). The circle is an experimental result for $x = 1$.

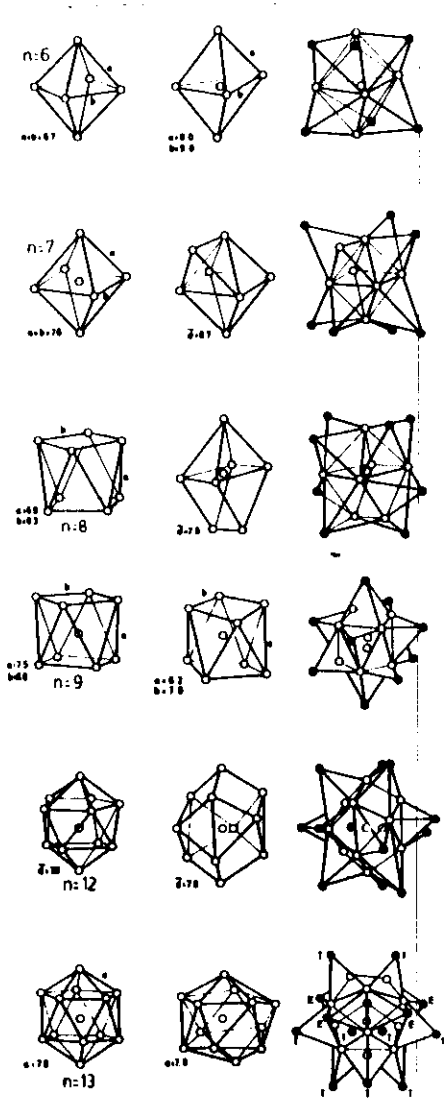

FIG. 10. Geometries of pure Na_n (left-hand column), Na_n part in Na_nCs_n (central column), and whole Na_nCs_n (right-hand column), for $n=6$, 7, 8, 9, 12, and 13. Open and solid circles represent Na and Cs atoms, respectively. Distances are all in a.u.